Springer

KSME

Journal of Mechanical Science and Technology 24 (12) (2010) 2561~2566
www.springerlink.com/content/1738-494x
DOI 10.1007/s12206-010-1001-4

# Numerical and experimental studies on characteristic surface temperature variations of aluminum plates facing different directions †

Jun-Hyuk Choi[1] and Tae-Kuk Kim[2,*]

[1]*Graduate school, Chung-Ang Univ., Seoul 156-756, Korea*
[2]*Dept. of Mechanical Engineering, Chung-Ang Univ., Seoul 156-756, Korea*

(Manuscript Received September 29, 2009; Revised March 31, 2010; Accepted October 7, 2010)

**Abstract**

This paper is a part of the work in developing a software that predicts IR signatures from objects in the scene by considering the direct and diffuse solar irradiations, the atmospheric convection and the conduction within objects. The thermal information of the objects and their background is essential for understanding the IR signature characteristics from the scene. The thermal contrast between the objects and the background is then used to obtain their infrared radiation contrast which is the important signal in identifying the objects. We considered the composite heat transfer modes including conduction, convection and spectral solar irradiation on the objects within a scene to calculate the surface temperature distribution. The radiative energy components included in the thermal analyses are consisted of the direct and diffuse solar irradiances and sky thermal irradiation, while the thermal conduction within the object is approximated as one-dimensional heat transfer into the depth. The measured diurnal surface temperature variations on the three different test plates facing east, south and west respectively are fairly well compared with the modeled results obtained from the software developed in this study and a commercial software. A complete set of measured data including the plate temperature together with the detailed weather information and the irradiation data can be valuable reference for future study.

*Keywords*: IR signature; Solar irradiation; Spectral surface property; Transient surface temperature; Silhouette

## 1. Introduction

Electromagnetic thermal radiation emitted from objects above 0 degree Kelvin can be utilized for many different purposes. The thermal radiation is a typical passive signal from the objects within a scene which can be detected covertly by some proper detectors located at a sufficient distance from them such as infrared detectors. The infrared signals from the objects propagate through semi-transparent media such as air, gas, liquid, or solid with some attenuation due to the absorbing and scattering characteristics of the media. Detection of these infrared signals from the objects lets us to figure out their appearances and movements even in the dark night [1, 2].

We are encouraged to utilize software tools to get the spectral infrared images from some specific remote objects for pre-examination purposes because it may not be a sufficient way to obtain the desired infrared data from those objects by measurement only due to a large variety of objects, environments, and meteorological conditions. However a few of the developed countries have the capabilities to develop, test and maintain the infrared image generation software which can be used to simulate the infrared signatures from the objects within a certain designated region [3, 4]. Some of the well-known software are DIRSIG (USA, [5]), RadThermIR or MUSES (USA, [6]), OKTAL-SE (France, [7]), ShipIR/NTCS (Canada, [8]) etc. These software are open to the public with limited functions and also they are very expensive even with the limited functions. These software tools can be used for synthetic image generation which includes simulated imagery in the visible through thermal infrared regions. They are designed to produce spectral imagery with band approximations through the integration of radiation propagation sub models.

This study is focused on experimentally verifying the thermal module of the synthetic infrared image generation software, Silhouette, developed by the authors. Three sets of test plates fabricated by using aluminum plates insulated on the back side are used to measure the diurnal temperature variations of the three plates facing east, south and west respectively. The diurnal variations of meteorological data including the solar and sky irradiations, the air temperature, the wind velocity and the wind direction are also measured at the same time interval as the temperature measurement. The measured diurnal surface temperatures are compared with those obtained by using the software developed in this study (Silhou-

† This paper was recommended for publication in revised form by Associate Editor Dongsik Kim

* Corresponding author. Tel.: +82 2 820 5282, Fax.: +82 2 814 9476
E-mail address: kimtk@cau.ac.kr

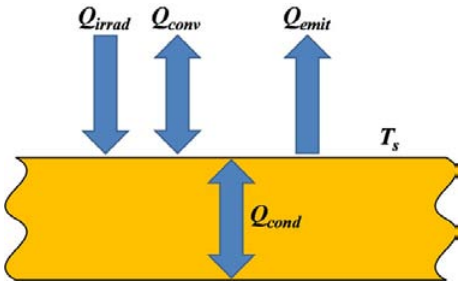


Fig. 1. Schematic diagram of the thermal balance on an object surface.

ette) and by using the commercial software (RadThermIR) where both of the modeled results are obtained by using the measured irradiation and weather data.

## 2. Theoretical background

The surface temperature of an object can be determined by considering the energy balance over a finite surface element as shown in Fig. 1. The resulting equation for the time-dependent surface temperature $(T_s)$ is expressed as [9, 10]

$$M_s C_{p,s}\left(\frac{dT_s}{dt}\right) = Q_{cond} + Q_{conv} - Q_{emit} + Q_{irrad} \tag{1}$$

where $M_s$ and $C_{p,s}$ are the mass and specific heat of the surface element. $Q_{cond}$ is the conductive heat transfer through the plate thickness (one-dimensional). $Q_{conv}$ is the convective heat exchange with the wind and $Q_{emit}$ is the surface emission [11]. $Q_{irrad}$ is the solar and sky energy absorbed by the surface. $Q_{irrad}$ is determined by considering the surface absorption as;

$$Q_{irrad} = \alpha_{ss} \cdot A_s \cdot \cos\theta_p \left(q_{solar,direct} + q_{solar,diffuse}\right) + \alpha_{sl} \cdot A_s \cdot \cos\theta_p \cdot q_{sky} \tag{2}$$

where $q_{solar,direct}$ and $q_{solar,diffuse}$ are the total solar energy fluxes by direct and diffuse irradiations. $q_{sky}$ is the total energy flux by the sky radiation. $\theta_p$ is the angle between the normal directions of object surface and the horizontal surface. The absorptivity $\alpha_{ss}$ is the hemispherical short-wave absorption property on the spectral band between 0.3-3 $\mu m$, and the absorptivity $\alpha_{sl}$ is the hemispherical long-wave absorption property on the spectral band between 3-30 $\mu m$ [12]. The two different spectral bands are considered since the solar energy flux meters used in this study detect the solar energy in these spectral bands respectively.

**Direct solar heat flux:** The total direct solar irradiation incident to the object surface can be calculated by integrating the spectral direct solar irradiation between the wavelength range 0~3 $\mu m$ as;

$$q_{solar,direct} = \int_0^3 \tau_s(\lambda) \cdot I_{solar,direct}(\lambda) \cos\theta_s \, d\lambda \tag{3}$$

where $I_{solar,direct}(\lambda)$ is the direct spectral solar intensity above the atmosphere. $\theta_s$ is the solar angle measured from the normal axis on the horizontal surface. $\tau_s(\lambda)$ is the atmospheric spectral transmission along the solar energy path. The total direct solar irradiation $q_{solar,direct}$ can also be measured by using a proper solar direct flux meter with sun tracker.

**Diffuse solar heat flux:** The total hemispherical diffuse solar irradiation can be calculated by integrating the spectral diffuse solar irradiation between the wavelength range 0~3 $\mu m$ as

$$q_{solar,diffuse} = \int_0^3 \int_0^{2\pi} \int_0^{\pi/2} \tau_i(\lambda) \cdot I_{solar,diffuse}(\lambda,\theta,\phi) \, d\theta \, d\phi \, d\lambda \tag{4}$$

where $I_{solar,diffuse}(\lambda,\theta,\phi)$ is the spectral diffuse solar intensity. $\theta$ and $\phi$ are the polar and azimuth angles. The total hemispherical diffuse solar irradiation $q_{solar,diffuse}$ can also be measured by using a proper solar diffuse flux meter. $\tau_i(\lambda)$ is the atmospheric spectral transmission along the atmospheric energy path.

**Sky heat flux:** The total hemispherical sky irradiation incident to the object surface can be calculated by integrating the spectral sky irradiation between the wavelength range 3~30 $\mu m$ as

$$q_{sky} = \int_3^{30} \int_0^{2\pi} \int_0^{\pi/2} \tau_i(\lambda) \cdot I_{sky}(\lambda,\theta,\phi) \, d\theta \, d\phi \, d\lambda \tag{5}$$

where $I_{sky}(\lambda,\theta,\phi)$ is the spectral diffuse sky intensity. The total hemispherical sky irradiation $q_{sky}$ can also be measured by using a proper sky flux meter.

## 3. Experimental validation

Surface temperature profile over the objects exposed to the atmosphere can be measured fairly accurately by using thermocouples installed on the object surface. The experimental validation of the software developed in this study can be more effective if we measure the solar and sky irradiations and the weather data at the same time when the surface temperatures are measured. By using the time dependent solar and sky irradiations and the weather data measured near the test plates, the validation procedure of the thermal module developed in this study can be free from the uncertainties due to the modeled solar and sky irradiations using the well-known softwares such as LOWTRAN [13] or MODTRAN [14]. In this study, we used three sets of simple test plates facing east, south and west directions with 15 degrees of inclined angle, and the weather station and the solar and sky irradiation measurement system are installed near the test plates as shown in Fig. 2. The Experimental site is located in Seoul, South Korea, at the latitude of 37.34N and the longitude of 126.34E.

Table 1. Accuracy of the weather station sensors.

| Weather Parameters | Unit | Accuracy |
|---|---|---|
| Wind velocity | m/s | ±0.3 m/s |
| Wind direction | Degree | ±2 ˚ |
| Atmospheric temperature | ℃ | ±0.3℃ |
| Relative humidity | % | ±3% |
| Atmospheric pressure | mbar | ±0.15 mbar |

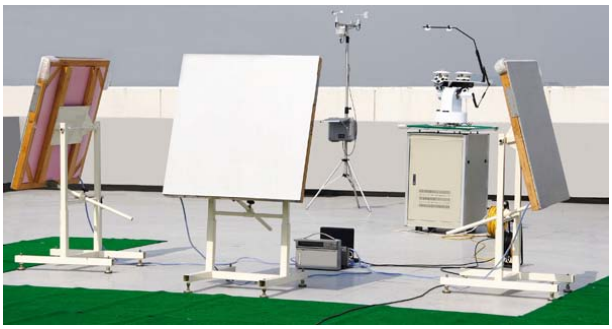

Fig. 2. Picture of the experimental system.

### *3.1 Test plates*

Three sets of test plates are fabricated by using aluminum plates with the dimensions of width [1 m] × length [1 m] × thickness [5 mm], and on the back side of each test plate thermal insulation board of 65 mm thick consisted of polyvinyl sponge sheet, polystyrene foam board and wood plate is applied as shown in Fig. 3. The heat conduction on the aluminum plate can then be approximated as one-dimensional mode through the plate thickness. On each of the aluminum plate 21 thermocouple sensors are mounted on the back side surface through the drill holes with the depth of 4mm as shown in Fig. 3. Each of the thermocouple sensors is inserted into the corresponding drill hole and mounted firmly by filling the copper based thermally conducting cement (Technovit 5000 from Kulzer Co. Ltd) into the hole. The uniformity of temperature on each of the test plates is checked by comparing the thermocouple readings from the 21 sensors. The maximum temperature difference between different sensors on each of the test plates is measured within 1°C which ensures that the heat conduction within the test plate is nearly one dimensional.

The time dependent temperature change on each of the test plates is then obtained by averaging the temperature values from the five thermocouple sensors located near the center of the test plate. A data logger with 60 channels (DC 100 from Yokogawa Co. Ltd) is used to gather the temperature values from 15 sensors on three test plates at every five minutes.

### *3.2 Weather station*

A portable weather station (NOMAD from Casella Co. Ltd) is used to measure the weather data near the test plates as shown in Fig. 2. Accuracy of each sensor mounted on the weather station is summarized as shown in Table 1. Five different weather data including the air temperature, wind velocity, wind direction, humidity and atmospheric pressure are recorded every five minutes during the experiment.

Table 2. Integrated irradiation flux instrument.

| Flux Parameters | Unit | Sensitivity |
|---|---|---|
| Pyrheliometer (NIP) | $W/m^2$ | Approx. 8 $\mu V/Wm^{-2}$ |
| Pyranometer (PSP) | $W/m^2$ | Approx. 9 $\mu V/Wm^{-2}$ |
| Pyrgeometer (PIR) | $W/m^2$ | Approx. 4 $\mu V/Wm^{-2}$ |

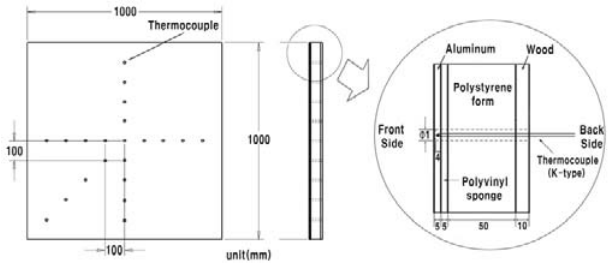


(a) Drawing of the test plate

(b) Test plate with the mounting device Test plate used for experiments

Fig. 3. Test plate used for experiments.

### *3.3 Integrated irradiation flux instrument*

The irradiation flux measurement is conducted by using the integrated irradiation sensor apparatus supplied by Epply Laboratory as shown in Fig. 2 which is mounted on the sun tracker. The irradiation flux sensors mounted on the sun tracker are consisted of the solar direct irradiation sensor (Normal Incidence Pyrheliometer (NIP) from EPLAB), the solar diffuse irradiation sensor (Precision Spectral Pyranometer (PSP) from EPLAB) and the sky irradiation sensor (Precision Infrared Radiometer (PIR) from EPLAB), and the accuracies of these sensors are summarized in Table 2. The irradiation data are recorded at the same time interval (every five minutes) as the temperature recording during the experiment.

Table 3. Material Properties considered[15].

| Material | Density ($kg/m^3$) | Specific heat ($J/Kg \cdot K$) | Thermal conductivity ($W/m \cdot K$) | Shortwave Absorptivity (0.3~3 $\mu$m) | Longwave Absorptivity (3~30 $\mu$m) |
|---|---|---|---|---|---|
| Aluminum | 2770.0906 | 884.2521 | 201.0733 | 0.30 | 0.22 |

## 4. Results and discussions

### *4.1 Applied conditions*

To validate the software developed in this study, the temperatures measured from the test plates are compared with those obtained from the modeling where the irradiation and weather data are supplied by the measurement. The test plates are located at the geographical location at the latitude of 37.34N and the longitude of 126.34E as described in Section 3, and the experiment was performed between August 27 and 28, 2008. The thermodynamic and optical properties of the aluminum considered in this study are listed in Table 3 [15].

### *4.2 Validation of the software*

The software developed in this study, Silhouette, is based on one dimensional heat conduction through the depth of the object. The temperature distribution is predicted by considering the solar and sky irradiations, the convection heat exchange with the atmosphere, and the heat conduction through the object. A well-known commercial software, RadThermIR, which is based on a fully three dimensional heat conduction model predicting the surface temperature distribution over the object surface is also used for comparison. The environmental parameters required by the RadThermIR and the Silhouette are provided by the measured data from the weather station and the irradiation flux instrument. The material properties of the aluminum plate given in Table 3 are used for the numerical modeling by the RadThermIR and the Silhouette.

Fig. 4 shows the diurnal cycle of the measured solar and sky irradiances, the atmospheric air temperature, the wind velocity, the wind direction, the relative humidity and the atmospheric pressure. Since the weather on the day of the experiment showed clear sky in the morning and showed some scattered clouds in the afternoon, the measured solar irradiation curve shows strong and smooth solar flux distributions in the morning and reduced solar flux distributions due to the scattered cloud in the afternoon. The solar irradiations are detected after 6:30 in the morning and are not detected after 6:30 in the afternoon, while the diffuse sky irradiation remains nearly unchanged during the whole cycle of the experiment. The air temperature and wind speed are also shown in Fig. 4, and the diurnal cycle variations of the air temperature, wind speed and direction are observed between 20 and 25℃, 0 and 4 m/s, 0 and 359°(0° indicates north direction and 90° indicates east direction) respectively.

Figs. 5, 6 and 7 show the diurnal cycle of measured and predicted surface temperatures of the plates facing east, south and west respectively shown together with the solar irradiations.

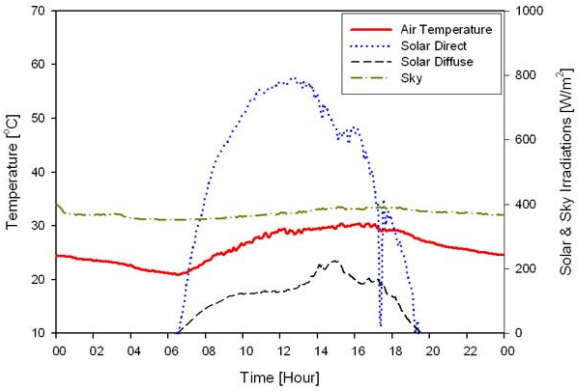


(a) Air temperature and irradiations

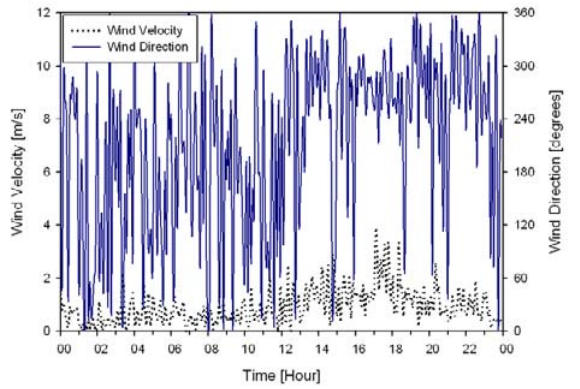


(b) Wind velocity and wind direction

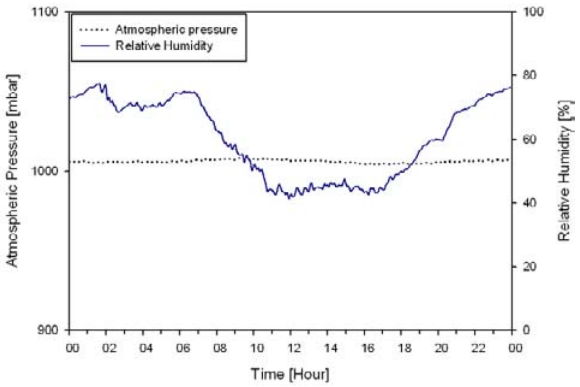


(c) Atmospheric pressure and Relative Humidity

Fig. 4. Measured diurnal solar and sky irradiations shown with the weather data.

Fig. 5 shows the diurnal temperature variations on the east facing plate obtained from the experiment and from the numerical predictions by using the Silhouette and the RadThermIR. All of the three different results show reasonable temperature variation curves reflecting the strong direct sun light before the noon and no direct sun light due to shade in the afternoon. The RadThermIR and the Silhouette predict temperature jump by the sunrise near 6:30 in the morning similar those shown by the experiment near 6:30 in the morning. The RadThermIR underpredicts the plate temperature in the period

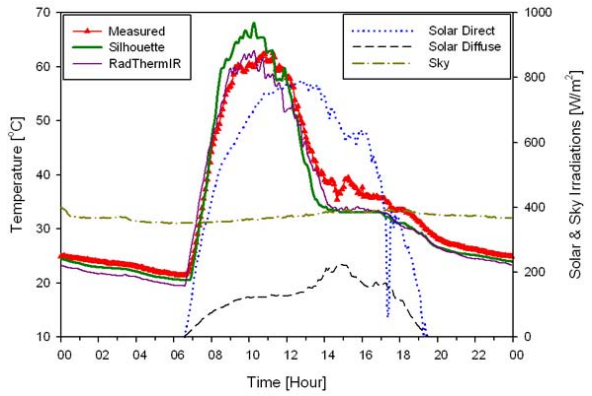


Fig. 5. Comparison of the measured and simulated diurnal plate temperatures shown with the irradiations (east facing with 15 degrees of inclined angle).

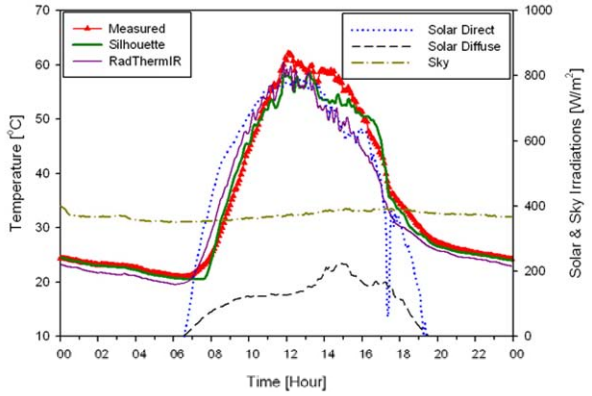


Fig. 6. Comparison of the measured and simulated diurnal plate temperatures shown with the irradiations (south facing with 15 degrees of inclined angle).

of no sun light up to 2.58℃ as compared to those obtained by the experiment and the Silhouette while the Silhouette over predicts the peak temperature due to the sun light near 10:00 in the morning than those obtained by the experiment and the RadThermIR. Both the RadThermIR and the Silhouette predict lower temperature profiles after 2:00 in the afternoon than those obtained from the experiment.

Fig. 6 shows the diurnal temperature variations on the south facing plate obtained from the experiment and from the numerical predictions by using the Silhouette and the RadThermIR. All of the three different results show reasonable temperature curves reflecting the strong direct sun light between 8:00 in the morning and 5:00 in the afternoon. The RadThermIR predicts earlier temperature rise due to the sun light in the morning and earlier temperature drop due to the sun set in the late afternoon as compared to the experiment and the Silhouette, and it also shows appreciable under prediction of the plate temperature up to 8.35℃ lower temperature as compared to the experiment especially in the afternoon. On the other hand, the Silhouette shows fairly reasonable results with less than 5.32℃ difference as compared to the experiment.

Fig. 7 shows the diurnal temperature variations on the west

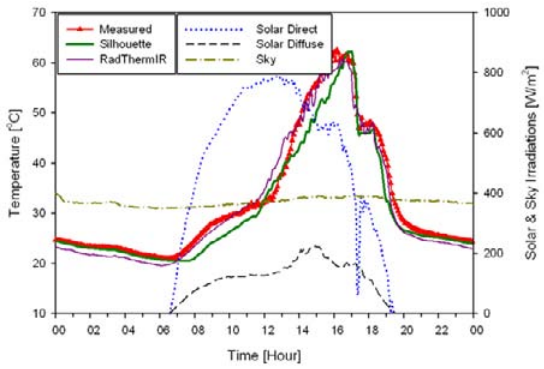


Fig. 7. Comparison of the measured and simulated diurnal plate temperatures shown with the irradiations (west facing with 15 degrees of inclined angle).

facing plate obtained from the experiment and from the numerical predictions by using the Silhouette and the RadThermIR. All of the three different results show reasonable temperature curves reflecting the strong direct sun light after the noon and the sun set near 6:30 in the afternoon. Although the RadThermIR shows appreciable underpredictions of the night time plate temperature, it shows fairly good agreements with the experimental temperature distributions while the Silhouette shows appreciable delay in temperature rise due to the sun light.

## 5. Conclusions

This study concludes that the modeling tools for prediction of the object surface temperature exposed to the atmosphere are useful for many applications. The two modeling tools used for demonstration of the surface temperature prediction, a commercial software RadThermIR and the Silhouette developed in this study, result in a fairly good agreement with the carefully measured surface temperature. For the thin flat aluminum plate the one-dimensional approximation for the conduction within the object can be a good approximation to reduce the computation time up to approximately 1/3 with minor loss of accuracy as compared to the well-known three-dimensional code, RadThermIR. Although the one-dimensional approximation for the conduction within the object can be a good choice for wide and flat objects the full three-dimensional modeling may be better selection for most of the objects with unequal heating by various internal and/or external heat sources. A complete set of measured data including the plate temperature together with the detailed weather information and the irradiation data supplied by this study can be a valuable reference for future study.

## Acknowledgements

This work has been supported by the Low Observable Technology Research Center program of Defense Acquisition Program Administration and Agency for Defense Development.

## Reference

[1] Jun-Hyuk Choi and Tae-Kuk Kim, Study on the spectral transmission characteristics of MWIR through the atmosphere, *Proc. Of SPIE*, image and signal processing for the remote sensing XIII, 6748 (2007).

[2] Vikram Dhar and Zafar Khan, Comparison of modeled atmosphere-dependent range performance of long-wave and mid-wave IR imagers, *Infrared Physics & Technology* 51 (2008) 520-527.

[3] Feng Weiwei and Wei qingnong, A scatterometer for measuring the polarized bidirectional reflectance distribution function of painted surfaces in the infrared, *Infrared Physics & Technology* 51 (2008) 559-563.

[4] Stefan Datcu, Laurent Ibos, Yves Candau and Simone Mattei, Improvement of building wall surface temperature measurement by infrared thermography, *Infrared Physics & Technology* 46 (2005) 451-467.

[5] DIRSIG , http://dirsig.cis.rit.edu/

[6] RadThermIR, http://www.thermoanalytics.com

[7] OKTAL, http://www.oktal-se.fr

[8] ShipIR/NTCS, http://www.wrdavis.com

[9] Jun-Hyuk Choi and Tae-Kuk Kim, Analysis of the spectral surface radiance by using the surface BRDF and atmospheric transmission effects, *Proc. Of SPIE*, Astronomical Instrumentation, 7017 (2008).

[10] Jun-Hyuk Choi and Tae-Kuk Kim, Study on spectral transmission characteristics of the reflected and self-emitted radiations through the atmosphere, *IEEE Multisensor Fusion Integration for Intelligent system* (2008).

[11] Pieter A. Jacobs, Thermal Infrared Characterization of Ground Targets and Background, *SPIE PRESS*, Bellingham, Washington USA, 2006.

[12] Alain Le Goff, Ph. Kersaudy, Jean Latger, Thierry Cathaka, Nilo Stolte and Ph. Barillot, *Proc. Of SPIE*, Target and Backgrounds VI, 4029 (2000).

[13] Neizys, F. X., Shette, L. W. Abreu, J. H. Chetwynd, G. P. Anderson, W. O. Gallery, J. E. A. Selby and S. A. Clough, Users Guide to LOWTRAN7, *Environmental Research Papers*, No. 1010 (1988).

[14] P. K. Acharya, A. Berk, G. P. Anderson, N. F. Larsen, S-Chee Tsay and K. H. Stammes, MODTRAN4: Mutiple Scattering and Bi-Directional Reflectance Distribution Function(BRDF) Upgrades to MODTRAN, *Proc. Of SPIE*, Optical Spectroscopy Techniques and Instrumentation of Atmospheric and Space Research, 3756 (1999).

[15] Image Mapper, http://www.surfaceoptics.com

**Jun-Hyuk Choi** received his M.S. and Ph.D. in the school of Mechanical Engineering from Chung-Ang University, Korea, in 2004 and 2009, respectively. His research interests include IR image generation and IR signatures analysis.

**Tae-Kuk Kim** received his M.S. in the school of Mechanical Engineering from Korea Advanced Institute of Science and Technology, Korea, in 1979. He received M.S. and Ph.D. in Mechanical Engineering from University of Minnesota, United States of America in 1986 and 1990, respectively. His current research interests are combined heat transfer and radiative energy transmission.